# EFFECT OF VENC ON ACCURACY OF VELOCITY PROFILES IN MULTI-SLICE PHASE-CONTRAST MR IMAGING OF STENOTIC FLOW

*MJ Negahdar[1], J. Cha[1], M. Shakeri[2], M. Kendrick[4],M. Alshaher[4], I. Khodarahimi[1],M. K. Sharp[2], A. Yancey[4], J. Heidenreich[3], and A. Amini[1]*

[1]Medical Imaging Lab, Dept. of Electrical and Computer Engineering,[2]Biofluid Mechanics Laboratory, Dept. of Mechanical Engineering, [3]Dept. of Radiology, University of Louisville, Louisville, KY[4]Robley Rex VA Medical Center, Louisville, KY

**ABSTRACT**

Phase-contrast MRI (PC MRI) is a powerful technique for imaging the flow velocities in-vivo. In PC MRI, the velocity encoding parameter, $V_{enc}$, plays a central role in fidelity of velocities acquired with this technique. Typically $V_{enc}$ is chosen to be the highest velocity in the flow. However, when acquiring velocity images at a number of slice locations, it may be advantageous to change the $V_{enc}$ as a function of position. The goal of this study was to determine the effect of $V_{enc}$ on the accuracy of the estimated velocity profiles in a range of locations in a phantom model of a 90% area stenosis. To this end, velocities from PC MRI were compared with velocities from computational fluid dynamics (CFD) simulations for identical geometry and flow conditions**.** Our results confirm that although using smaller $V_{enc}$'s leads to wrapping artifact, it provides more accurate velocity profiles. However, there is a lower limit to setting the $V_{enc}$, beyond which phase-unwrapping becomes uncertain.

***Index Terms***— *Phase-Contrast MRI, Computational fluid dynamics, $V_{enc}$, Atherosclerotic Disease, phase unwrapping*

## *1. INTRODUCTION*

The use of phase contrast to determine fluid velocities was first proposed by Hahn in 1960 [1]. The first application of this method in imaging was developed by Moran [2], and subsequently applied in human cases by Van Dijk [3]. The basis of the phase contrast technique is that spins moving in the presence of a magnetic field gradient acquire a different cumulative phase than stationary spins. For a spatial position vector $r(t)$, and a magnetic field gradient vector $G(t)$, the cumulative phase of the spins in the rotating frame is given by

$$\varphi(t) = \gamma \int_0^t G(\tau).r(\tau)d\tau \quad (1)$$

where γ is the gyromagnetic ratio. For simplicity, let us assume that the motion and the gradient are both in the x direction, substituting a second-order Taylor' expansion of the general equation for a spin's position, x(t), equation (1) becomes

$$\varphi(t) = \gamma x_0 \int_0^t G_X(\tau)d\tau + \gamma v_X \int_0^t G_X(\tau).\tau d\tau + \gamma \frac{1}{2} a_X \int_0^t G_X(\tau).\tau^2 d\tau \quad (2)$$

With $M_n$ representing the nth moment of the gradient waveform and $V_x$ the velocity in x direction, equation (2) becomes

$$\varphi(t) = \gamma\{x_0 M_0 + v_X M_1 + \frac{1}{2} a_X M_2\} \quad (3)$$

Therefore, flow dependent cumulative phase shift depends on initial position, velocity, acceleration, and higher order terms through the gradient's zeroth, first, second, and higher order moments, respectively. If we assume $x_0 = 0$, $a_x = 0$ (constant velocity) and assume higher order terms to be zero, we can rewrite cumulated phase in equation (3) as follows:

$$\varphi = \gamma v_X M_1 \quad (4)$$

$$v_X = \frac{\varphi}{\gamma M_1} \quad (5)$$

By measuring cumulative phase of the spins, it is possible to extract velocity by using equation (5). To remove signal from static tissue and noise, two separate scans with identical gradient zero time-moments and different first time-moment can be subtracted. Therefore, to construct a velocity image two separate scans are needed. Phase values that are greater than $\pi$ radians cannot be discriminated from their modulus $2\pi$ counterparts, so the velocity corresponding to a phase-shift of $\pi$ radians defines the upper limit and $-\pi$ the lower limit of the range of velocities that can be accurately measured. It is convenient to define

$$V_{enc} = \frac{\pi}{\gamma \Delta M_1} \quad (6)$$

In that case, the maximum measureable velocity maps to a phase shift of $\pi$ radians. Any velocity value outside of the range [-Venc +Venc] will be aliased and assigned to a smaller value due to wrapping nature of phase. The upper

limit of this range is referred to as the velocity encoding value or $V_{enc}$ [4, 5]. It is advantageous to set $V_{enc}$ as small as possible because decreasing $V_{enc}$ results in better velocity resolution and lower noise [6, 7]. The relationship between the standard deviations of phase noise and velocity noise is

$$\sigma_v = \frac{V_{enc}}{\pi}.\sigma_\varphi \qquad (7)$$

Therefore, to increase velocity resolution, decrease noise and avoid the aliasing issue, the commonly adopted approach is to set $V_{enc}$ slightly higher than the maximum velocity in the flow. An additional issue to consider is that smaller $V_{enc}$'s result in better velocity resolutions. One possible approach to reducing noise and having better velocity resolutions is to choose a $V_{enc}$ lower than the maximum velocity in the flow. This will lead to velocities being aliased, requiring a further phase unwrapping as a correction step. While using a constant value for $V_{enc}$ throughout the imaging volume is conventional, increased velocity resolution may be possible by varying $V_{enc}$ depending on the location of the imaged slice.

In this study, we considered the challenging scenario encountered in PC MRI imaging of stenotic flow. In the setting of a vascular stenosis, one encounters parabolic velocity profiles proximal to a stenosis, plug flow at the throat of the stenosis, and jet flow distal to the stenosis with an annular recirculation zone exhibiting negative velocities. The goal of this study was to determine the effect of a variable $V_{enc}$ strategy on the accuracy of the estimated velocity profiles at a range of locations in a phantom model of a vascular occlusion.

## 2. MATERIALS AND METHODS

### 2.1. Stenotic Vessel Phantom

Experiments were carried out using a closed loop flow system (Figure 1). A CardioFlow 1000 programmable pump (Shelley Medical Imaging Technologies, London, Ontario, Canada) was used for generating flows of a range of waveforms with less than 1% variance. The upstream steady flow rate generated using the pump was 46.4 ml/s, corresponding to Reynolds numbers of 160 at the inlet and 506 at the stenosis throat, respectively, which are within the range of Reynolds numbers observed in the common iliac artery.

An idealized rigid model of axisymmetric Gaussian shape was machined from transparent acrylic using conventional CNC machining methods initially aimed at 90% area occlusion. Later, the exact geometry was measured with high-resolution CT scans ($0.22 \times 0.22 \times 0.625\, mm^3$) and the area occlusion was found to be 87%.There were additional imperfections in fabrication of the phantom which caused the phantom geometry to not be completely axi-symmetric. The stenosis diameter narrowed from 25.4 mm

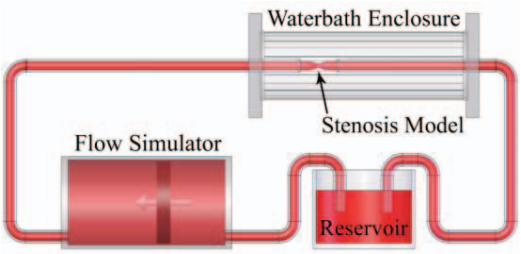



Fig.1. Schematic of the experimental setup showing the solid model of the 87% area stenosis which was machined in-house from clear acrylic plastic.

at the inlet to 9.04 mm at the throat. To ensure fully developed laminar flow at the entrance of the model, a 75-cm long straight rigid acrylic tube was placed upstream of the test section. The experimental system was designed to allow one to easily swap-in any precision-machined vascular model of matching diameter at entrance and exit inside the water-bath enclosure (Figure 1).

The viscosity of the blood-mimicking solution utilized in the MRI experiments was measured using a LVT Cone-Plate viscometer (Brookfield Labs., Stoughton, MA, USA) to be 0.022 Pa.s at 68°F. The density of the solution was 1600 kg/m$^3$. The solution had a T1 and T2 value of 500 ms and 45 ms, respectively, at a main field of 3T.

### 2.2. MRI Experiments

Imaging was performed on a Philips Achieva 1.5T scanner (Philips Healthcare, Best, NL). To measure the velocity, a multi-2D turbo gradient echo sequence was utilized that included bipolar velocity encoding gradient in a single predetermined direction. Conventional Cartesian trajectory was chosen for image acquisition. The remaining sequence parameters were as follows: FOV = 96x96 mm, 1.5x1.5 mm acquired in-plane resolution, 4mm slice thickness, flip angle = 5, turbo factor = 3, matrix size = 64x64, TR/TE = 7.6/4.5 (for $V_{enc}$ = 85 cm/s). In order to ensure good signal quality, an 8-element phased-array knee coil was used. The phantom was placed at the center of the knee coil and images were acquired at or close to the iso-center of the magnet.

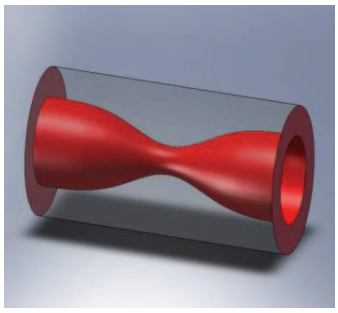
With the z = 0 location corresponding to the center of the stenosis, axial slices were collected at locations both proximal and distal to the stenosis. To ascertain the sensitivity of data accuracy to $V_{enc}$ values, each slice location was scanned 4 times with different $V_{enc}$ values in the FH (Foot-to-Head) direction. To determine the highest $V_{enc}$ for the flow, we scanned the phantom at z = 0 and determined the smallest $V_{enc}$ that did not alias the velocities. This approach lead to the minimum $V_{enc}$ = 85 cm/s for the site of stenosis at z = 0. Subsequently, we used $V_{enc}$ = 85, 65, 45, and 30 cm/sec at all axial locations as part of four different acquisitions – some of these $V_{enc}$'s lead to wrapped phase and aliased velocities in the flow.

### 2.3. CFD Simulation

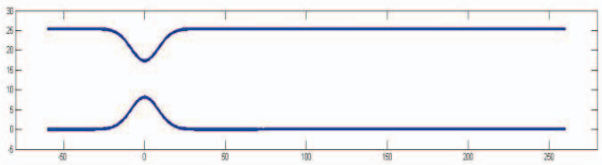
The flow was numerically simulated for the same flow rate, geometry, and fluid properties as in the PC-MRI experiments. The geometry of the simulated stenosis was set to match scans obtained on a 64-slice multi-detector CT scanner (LightSpeed VCT scanner, GE Medical Systems, Milwaukee, WI, USA) with slice thickness of 0.625 mm and in-plane resolution of 0.22 mm × 0.22 mm. Therefore, we can be certain that the "lumen" boundary created from CT was an exact replica of the continuous physical phantom up to the resolution of the CT system.

The geometry was created in the preprocessor, GAMBIT 2.4.6 (ANSYS, Inc., Canonsburg, PA, USA). Explicit grid refinements were performed until negligible changes in the final results were observed. The final mesh used in this study had 1,200,000 pyramid/wedge shaped computational cells. To better resolve the flow near the wall and in the neighborhood of the stenosis throat, the computational domain was meshed with a successive ratio of 1.2 from the wall towards the centerline of the phantom, and with a bell-shaped distribution in the stream-wise direction centered at the stenosis. The length of the computational domain was 17 diameters.

Velocity distribution over the phantom volume was computed by solving the 3D Navier-Stokes equations for an incompressible Newtonian fluid, with rigid walls using the CFD software package Fluent 12.1 (ANSYS, Inc., Canonsburg, PA, USA) based on a finite volume scheme. Figure 2 shows the stenotic phantom used in CFD simulation.



(a)



(b)

Fig.2. (a) 3D model of the stenotic phantom. (b) A sagittal cut through the phantom.

## 3. RESULTS

To compare velocity profiles from CFD simulations to those from MRI experiments, the CFD data was regridded onto a uniform grid and subsequently interpolation and decimation of the CFD data was performed to match the spatial resolution of PC MRI experiments.

Due to manufacturing imperfections noted earlier, the velocity profiles proximal to the stenosis were not completely symmetric around the z axis. As an example, Figure 3 demonstrates the regridded CFD velocity profile at z = -48 mm (proximal to stenosis). The peak of the velocity does not occur exactly at the center of the slice as would be expected for the completely axi-symmetric condition. Figure 4 demonstrates two registered MR and CFD image at identical slice, 48 mm distal to stenosis.

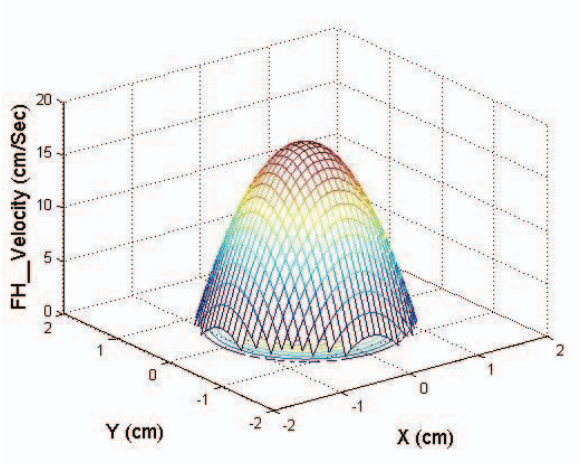



Fig.3. Regridded CFD velocity profile at slice 48mm proximal to the stenosis.

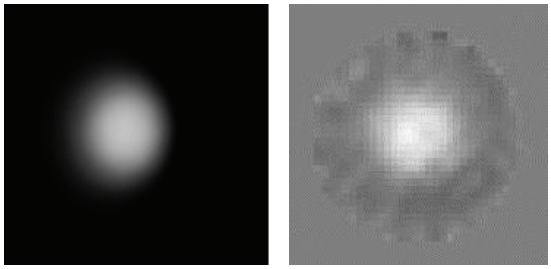


Fig.4. CFD and MR velocity images at z = 48 mm distal to stenosis.

As noted in section 2.2, the lower $V_{enc}$ values lead to aliased velocities for slices at z > 0. To overcome this issue we performed phase unwrapping to generate valid velocity profiles for all slices. However, severe aliasing was observed for $V_{enc}$ = 30 and this data set were therefore discarded. Figure 5 demonstrates the phase-unwrapping

process for slice location z = 24 mm. The cupping effect at the center of the slice is clearly visible which has been corrected on the right. The phase unwrapping approach involved detecting the sharp negative jump in intensity level around the aliased pixels. $2\pi$ was added to the phase of pixels' inside this contour, which is equivalent to adding $2*V_{enc}$ to the corresponding velocities.

$$\varphi_{Correct} = \varphi_{Aliased} + 2\pi \quad (8)$$

$$V_{Correct} = V_{Aliased} + 2*Venc \quad (9)$$

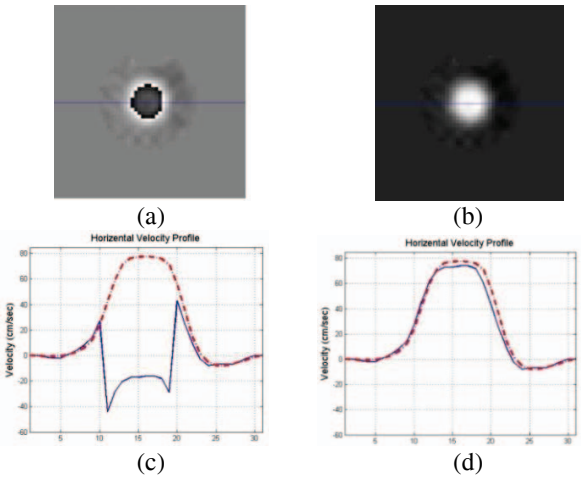



Fig. 5. (a) Aliased velocity image at z = 24 mm due to using small Venc (Venc = 45 cm/s), and (b) unwrapped phase image. (c), (d) velocity profiles along horizontal lines going through center of the image (solid line is PC MRI and dotted line is CFD).

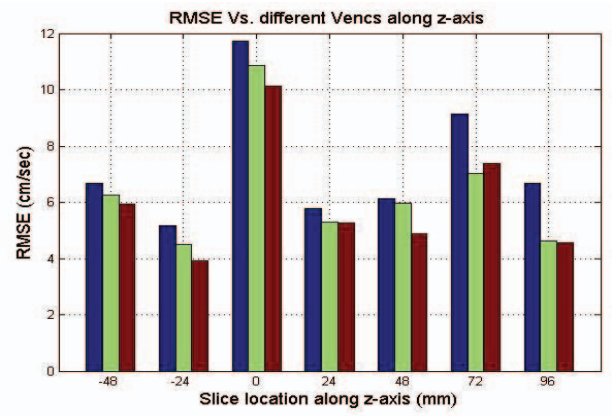



Fig.6. RMS error for different slices and different $V_{enc}$ values. $V_{enc}$ was 85 cm/s (blue),65 cm/s (green), and 45 cm/s (red) respectively from left to right. Slice locations were at z = -48, z = -24, z = 0, z = 24, z = 48, z = 72, and z = 96 mm respectively.

After performing unwrapping, we calculated 2-D RMS errors between CFD and MR velocities for two slices proximal to stenosis, one slice at the site of stenosis, and 5 slices distal to the stenosis (Figure 6).

## 4. DISCUSSION AND CONCLUSIONS

We investigated the effect of $V_{enc}$ on accuracy of velocity profiles in PC MR imaging of stenotic flow as part of a detailed phantom experiment. We used CFD simulation as reference velocity profiles.

Our results confirm that although using smaller $V_{enc}$'s leads to wrapping artifact, it provides more accurate velocity profiles. The drawback of course is that phase unwrapping needs to be applied to unwrap the phase and correct aliased velocities. There is however a lower limit to setting the $V_{enc}$ beyond which phase unwrapping becomes difficult. For the flow rate that we considered this was one-third of highest velocity in the flow.

Future work will include consideration of more complex and physiologic pulsatile flows.

## 5. ACKNOWLEDGMENTS

This work was supported in part by the National Science Foundation under Grant 0730467 and by an innovative grant from the Clinical and Translational Research Program of the University of Louisville to A. Amini.

## 6. REFERENCES

[1] E. L. Hahn, "Detection of Sea-Water Motion by Nuclear recession,"*Journal of Geophysical Research,* vol. 65, pp. 776-777, 1960.

[2] P. R. Moran, "A flow velocity zeugmatographic interlace for NMR imaging in humans,"*Magnetic Resonance Imaging,* vol. 1, pp. 197-203, 1982.

[3] P Van Dijk, "Direct Cardiac NMR Imaging of Heart Wall and Blood Flow Velocity,"*Journal of Computer Assisted Tomography,* vol. 8, pp. 429-436, 1984.

[4] N. J. Pelc, F. G. Sommer, K. C. Li, T. J. Brosnan R. J. Herfkens, and D. R. Enzmann, "Quantitative magnetic resonance flow imaging,"MagnReson Q, vol. 10, pp. 125-47, Sep 1994.

[5] D. G. Nishimura, P. Irarrazaval, and C. H. Meyer, "A velocity k-space analysis of flow effects in echo-planar and spiral imaging," MagnReson Med, vol. 33, pp. 549-56, Apr 1995.

[6] A. Nasiraei-Moghaddam, G. Behrens, N. Fatouraee, R. Agarwal, E. T. Choi, And A. Amini, "Factors affecting the accuracy of pressure measurements in vascular stenoses from phase-contrast MRI," Magnetic Resonance in Medicine, vol. 52, pp. 300-309, 2004.

[7] B. R. Haacke EM, Thompson M, Venkatesan R., Magnetic resonance imaging: physical principles and sequence design, John Wiley and Sons Inc., 1999.